Journal of Chemical Research and Innovation
ISSN: 3106-7905 | 3106-7891
Volume 3, Issue 1, 2026

ENHANCED ENVIRONMENTAL REMEDIATION USING $CeO_2/Zn_2V_2O_7$ HYBRID NANOCATALYSTS

Shazia Zahir[*1], Anjum Ihsan[2]

[*1,2]*Assistant Professor, Department of Chemistry, University of Lahore, Lahore, Pakistan*

[*1]shaziazahir20@yahoo.com,[2]anjumihsan12@gmail.com

Keywords
Zinc vanadate, Cerium oxide, Methylene blue, Photocatalysis, Wastewater treatment

Article History
Received: 01 January 2026
Accepted: 15 March 2026
Published: 31 March 2026

Corresponding Author: *
Shazia Zahir

Abstract

Toxic pollutants in wastewater present serious risks to both the environment and human health, highlighting the pressing need for efficient and sustainable remediation methods. Among the available techniques, photocatalytic degradation has emerged as an environmentally friendly and effective strategy for eliminating organic contaminants, especially synthetic dyes. In this study, a $CeO_2/Zn_2V_2O_7$ heterostructured nanocatalyst was synthesized through a coprecipitation method and evaluated for its photocatalytic performance in degrading methylene blue.The structural, optical, and morphological characteristics of the synthesized nanomaterials were examined using X-ray diffraction (XRD), UV–Visible spectroscopy, Fourier transform infrared (FTIR) spectroscopy, and scanning electron microscopy (SEM). The $CeO_2/Zn_2V_2O_7$ composite exhibited markedly superior photocatalytic efficiency compared to pure $Zn_2V_2O_7$, with the 50% CeO_2 composition achieving the highest degradation rate. This enhanced activity is attributed to improved charge carrier separation and increased redox capability, demonstrating the strong potential of CeO_2-based heterojunctions for advanced wastewater treatment applications.

1.INTRODUCTION

The economy and standard of living have improved due to the exponential rise in industrialization1. This process generates harmful contaminants, including heavy metals, radioactive nuclides, and organic pollutants2,3. These contaminants cause the water to smell and accumulate in aquatic life, allowing it to enter both animal and human bodies through the food chain4,5. Therefore, traditional methods for treating polluted water may not be very effective in breaking down these harmful contaminants6–8. Techniques such as biodegradation, flocculation, redox methods, and electrodeposition are examples of conventional wastewater treatment methods9–12. However, they have not been particularly effective at degrading these pollutants. Advanced oxidation processes (AOPs) represent a cutting-edge approach developed to tackle the challenge of remediating contaminants in organic wastewater and are believed to be highly efficient13. AOPs specifically target organic pollutants by generating reactive hydroxyl radicals and include methods like photo catalysis, Fenton-like reactions, and ozone oxidation14,15. AOPs that are photo catalytically active are often used to remove organic contaminants and dyes from industrial wastewater due to their safety, cost- effectiveness, eco-friendliness, and high efficacy16–22. Currently, various photo catalysts, particularly metallic oxide semiconductors, are utilized for wastewater treatment because they are easy to synthesize and stable during chemical reactions. Cerium, the first member of the lanthanide series, has garnered attention due to its 4f orbital being shielded by 5p and 4d electrons23. This

characteristic is significant for catalytic studies, and another advantage for selection is its existence in both +3 and +4 oxidation states23. Ceria, also known as cerium oxide (CeO2), is a metal oxide semiconductor widely used for degrading wastewater contaminants. Additionally, it finds applications in various industries, including solar cells, oxygen sensors, and fuel cells. Because of its reversible Ce+3/Ce+4 pairings, ceria demonstrates remarkable catalytic power, photo-corrosion resistance, and a high capacity for oxygen transport. Consequently, ceria is employed as a potent photocatalyst 24,25. Unfortunately, ceria's bandgap of 2.8-3.2 eV, which is high for photocatalysts, limits its applicability, as it primarily absorbs radiation in the UV range. Since visible light is less expensive, several techniques have been developed to reduce the bandgap for visible light utilization. CeO2-based nano-photocatalysts are commonly used for carbon dioxide conversion, water splitting, air purification, and pollutant photodegradation. Over the past decade, heterometal oxides, particularly vanadates, have gained attention for their versatile behavior in photocatalysis26–28. In this regard, zinc vanadates have gained particular importance due to their photocatalytic capability for utilizing visible light and their ability to treat waste materials with refractory pollutants29–33. Other advantages include low cost, non-toxic nature, appropriate band gap, charge mobility, unique hexagonal structure, and strong oxidation potential (0.3 eV) with high chemical stability34-36

In this study, we aim to synthesize a CeO2/Zn2V2O7 heterostructure using the coprecipitation method to enhance photocatalytic ability for the degradation of Methylene blue in sunlight. The synthesized material will be systematically characterized using XRD to confirm crystallinity, UV-Vis spectroscopy for bandgap analysis, FTIR for functional group identification, and SEM for morphological assessment. The photocatalytic performance will be evaluated to determine the efficiency of the composite compared to pure Zn2V2O7, focusing on charge carrier separation and redox processes. This work establishes CeO2-based heterostructures as promising candidates for advanced wastewater treatment applications.

1.EXPERIMENTAL

1.1. Chemicals

The chemicals used in this experiment, including cerium nitrate [Ce $(NO_3)_3$], ammonium metavanadate (NH_4VO_3), sodium hydroxide (NaOH), polyethylene glycol, and methylene blue ($C_{16}H_{18}N_3SCl$), were obtained from Sigma Aldrich and were employed without further purification.

1.2. Material Synthesis

Zinc vanadate is synthesized using a non-hydrothermal method. A 0.1 M solution of ammonium metavanadate (NH_4VO_3) was prepared by dissolving 2.23 g of NH_4VO_3 in 200 mL of distilled water. Separately, a 0.15 M solution of zinc nitrate was obtained by dissolving 8.91 g of zinc nitrate in 200 mL of distilled water. The two solutions were mixed dropwise at 70°C under continuous stirring for 30 minutes, resulting in the formation of a strongly orange-colored $ZnVO_x$ precipitate. The obtained sample was thoroughly washed, dried at 75 °C for 40 minutes, and subsequently annealed at 600 °C for 2 hours, yielding an orange-golden Zn2V2O7 powder.

For the synthesis of CeO2/ Zn2V2O7, a 0.2 M solution of cerium nitrate [Ce $(NO_3)_3$] was obtained by dissolving 4.3 g of Ce $(NO_3)_3$ in 50 mL of deionized water. To this solution, 2 mL of polyethylene glycol (C_2 n H $_4$ $n_{+2}O_{n+1}$) was added, followed by stirring for 30 minutes. Fine zinc vanadate powder was then introduced in varying amounts for different doping levels: 0.825 g for 10%, 1.704 g for 20%, 2.55 g for 30%, 3.4 g for 40%, and 4.26 g for 50%. For 30 minutes, the mixture was again stirred. A 1 M solution of sodium hydroxide (NaOH) was prepared by dissolving 2 g of NaOH in 50 mL of distilled water and was added dropwise to the cerium nitrate solution until the pH reached 9. The mixture was stirred for another 30 minutes, and the resulting precipitate was washed with ethanol, collected, and dried at

Journal of Chemical Research and Innovation
ISSN: 3106-7905 | 3106-7891
Volume 3, Issue 1, 2026

110 °C in an oven. The dried sample was then calcined at 480 °C for 2 hours, ground into fine particles, and stored for the next steps of analysis. A systematic illustration of the synthesis process is presented in Figure 1.

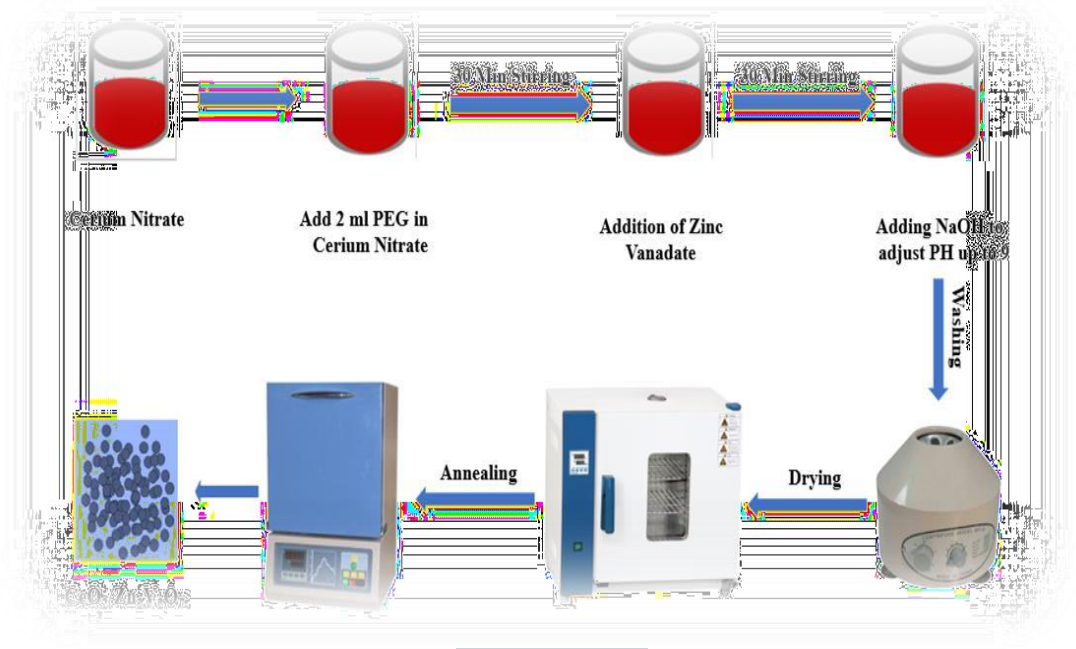

Figure 1. Schematic Illustration of CeO_2:$Zn_2V_2O_7$

1.1. Characterization

For characterization, various analytical techniques were employed. To ascertain the material's crystalline structure, X-ray diffraction (XRD) was performed using a Bruker D-8 X-ray diffractometer with Cu-Kα radiation (λ = 1.54 Å). The morphology of the surface was examined using a scanning electron microscope (SEM). Optical properties were analyzed through UV-visible spectroscopy using an LX211D Lab Dex double-beam spectrophotometer. Functional groups in the composite materials were identified using Fourier-transform infrared (FTIR) spectroscopy (PerkinElmer, L1600107).

1.2. Photocatalytic Activity

For the photocatalytic experiments, methylene blue ($C_{16}H_{18}ClN_3S$) was selected as a model pollutant for the catalytic degradation study. A 10-ppm methylene blue solution was prepared, and 0.1 g of the photocatalyst was added. The solution was continually swirled in the dark before irradiation to attain adsorption and desorption equilibrium between the dye and catalyst. By subjecting the solution to a 400 W halogen lamp, the photocatalytic reaction was started. Five-milliliter samples were taken out every ten minutes and subjected to UV-visible spectroscopic analysis to measure the efficiency of degradation.

The percentage degradation was calculated using the pseudo-first-order kinetic equation:

$$Degradation\ (\%) = \left(\frac{C_0 - C_t}{C_0}\right) \times 100$$

Journal of Chemical Research and Innovation
ISSN: 3106-7905 | 3106-7891
Volume 3, Issue 1, 2026

where C_0 represents the initial dye concentration, and C_t denotes the dye concentration at time t.

2. RESULT AND DISCUSSION

2.1. XRD Analysis

X-ray diffraction (XRD) analysis was performed to assess the phase purity and crystal structure of CeO2, Zn2V2O7, and their composites with varying Ce content (10–50 wt%). The XRD patterns, presented in the attached figures, confirm the structural characteristics of Zn2V2O7 (JCPDS Card # 00-029-1396), CeO2(JCPDS Card # 01-081-0792), and their hybrid composites. These materials contain Zn, V, O, and Ce elements, indicating the coexistence of zinc vanadate and cerium oxide within the composite structure (Figure 2). The XRD spectra exhibited four distinctive peaks, with two attributed to zinc vanadate, centered around 8000 eV. Additional peaks at 1021 eV and 1044 eV represent the 2D structure of Zn2V2O7$Zn_2V_2O_7$. In the CeO2 (40 wt%)/ Zn2V2O7 composite, a slight positive shift (~0.3 eV) was observed in the Zn 2p, V 2p, and O 1s peak positions compared to pure Zn2V2O7. This shift suggests a change in the chemical environment of Zn, V, and O, likely due to strong interfacial interactions between Zn2V2O7$Zn_2V_2O_7$ and CeO2, leading to the formation of the CeO2/ Zn2V2O7 heterojunction.

Figure 2. XRD Graph pattern of CeO2, Zn2V2O7 & their hybrid composites.

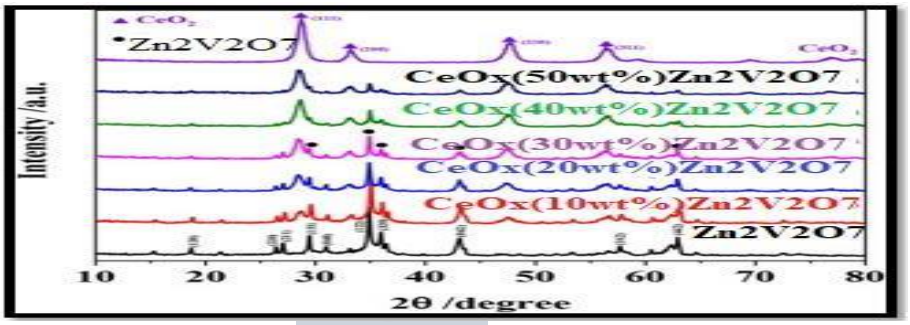

2.2. FTIR Analysis

Fourier Transform Infrared Spectroscopy (FTIR) analysis confirmed the formation of Zn2V2O7 and CeO2 phases, with characteristic peaks varying based on Ce incorporation. Pure Zn2V2O7 exhibited peaks at 828 cm^{-1} and 641 cm^{-1} (tetrahedral VO_4 vibrations), 3757 cm^{-1} (O-H stretching), and 493 cm^{-1} (Zn-O stretching). For pure CeO2 nanoparticles, key peaks included 1553 cm^{-1} (O-H bending/stretching of adsorbed water), 1356 cm^{-1}, 1055 cm^{-1} (=C-H in-plane vibration), and 862 cm^{-1} (Ce-O stretching). With increasing Ce content in Zn2V2O7, additional peaks appeared at 1636 cm^{-1} (H-O-H bond), 1370–1366 cm^{-1} (Ce-O-Ce and Ce-O stretching), 1154 cm^{-1} (Ce-O stretching), 1119–1123 cm^{-1} (Ce-O-Ce bond), 931–922 cm^{-1}, 828 cm^{-1}, 774 cm^{-1} (Zn-V bond), and 779–720 cm^{-1} (V-O-Zn and V-O-V modes). Hydroxyl groups were indicated by absorptions at 3776 cm^{-1}, 3742 cm^{-1}, and 3246 cm^{-1}. A gradual decrease in the 515 cm^{-1} peak suggested interfacial interactions between CeO2 and Zn2V2O7, while the V-O-V peak shifted lower with increasing Ce content, accompanied by the emergence of a peak at 563 cm^{-1}. These spectral variations confirm structural modifications due to Ce incorporation (Figure 3).

Journal of Chemical Research and Innovation
ISSN: 3106-7905 | 3106-7891
Volume 3, Issue 1, 2026

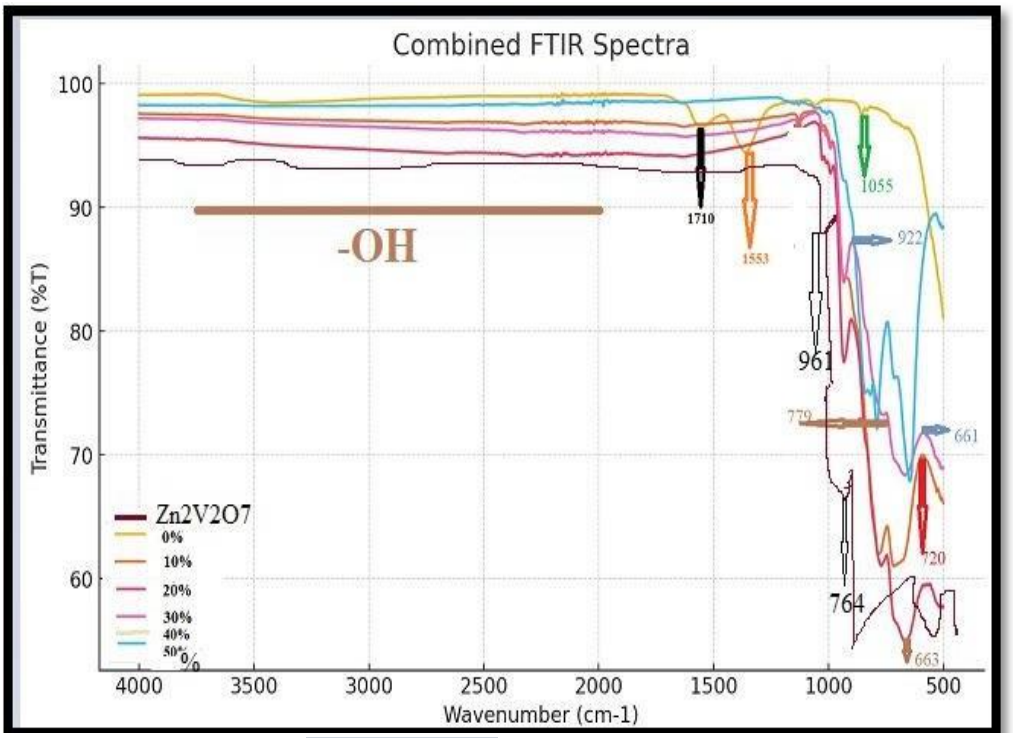

Figure 3. FTIR Spectra of CeO_2, $Zn_2V_2O_7$ and their composite.

2.3. Optical Analysis

UV-visible spectroscopy was performed to estimate the activation wavelength of Zinc Vanadate, Cerium Oxide, and Ce-doped Zinc Vanadate at varying concentrations. The band gap decreased to 2.1 V of 50% CeO_2/ $Zn_2V_2O_7$. The calculation of the optical band gap was achieved by using the Tauc plot method [37]. The equation $E = hc/\lambda$, where h is Planck's constant, c is the speed of light, and λ is the wavelength, is used to plot energy (E) on the x-axis. The y-axis represents the product of energy and the absorption coefficient, calculated using a corresponding equation. The UV-visible spectrum, shown in Figure 5, was used to derive these values.

2.4. Photocatalytic dye degradation

The photodegradation ability of the synthesized photocatalysts was evaluated using a 0.05 mM methylene blue solution as a model pollutant. Upon exposure to a solar irradiation lamp, the solution reached equilibrium, initiating the photodegradation process. Initially blue, the solution gradually faded to colourless, indicating degradation. To quantify this process, aliquots were extracted every 10 minutes and analysed via UV-visible spectroscopy to determine the remaining methylene blue concentration. Figure 6 illustrates the degradation of methylene blue by pure Zinc Vanadate, pure Cerium Oxide, and Ce-doped $Zn_2V_2O_7$ composites with varying Ce content (10–50%). A progressive decline in the absorption peak of methylene blue was observed at each interval, confirming degradation. Complete degradation of 50% CeO_2/ $Zn_2V_2O_7$, i.e., 92%, occurred within 90 minutes, as evidenced by the transition from blue to a colourless solution.

Journal of Chemical Research and Innovation
ISSN: 3106-7905 | 3106-7891
Volume 3, Issue 1, 2026

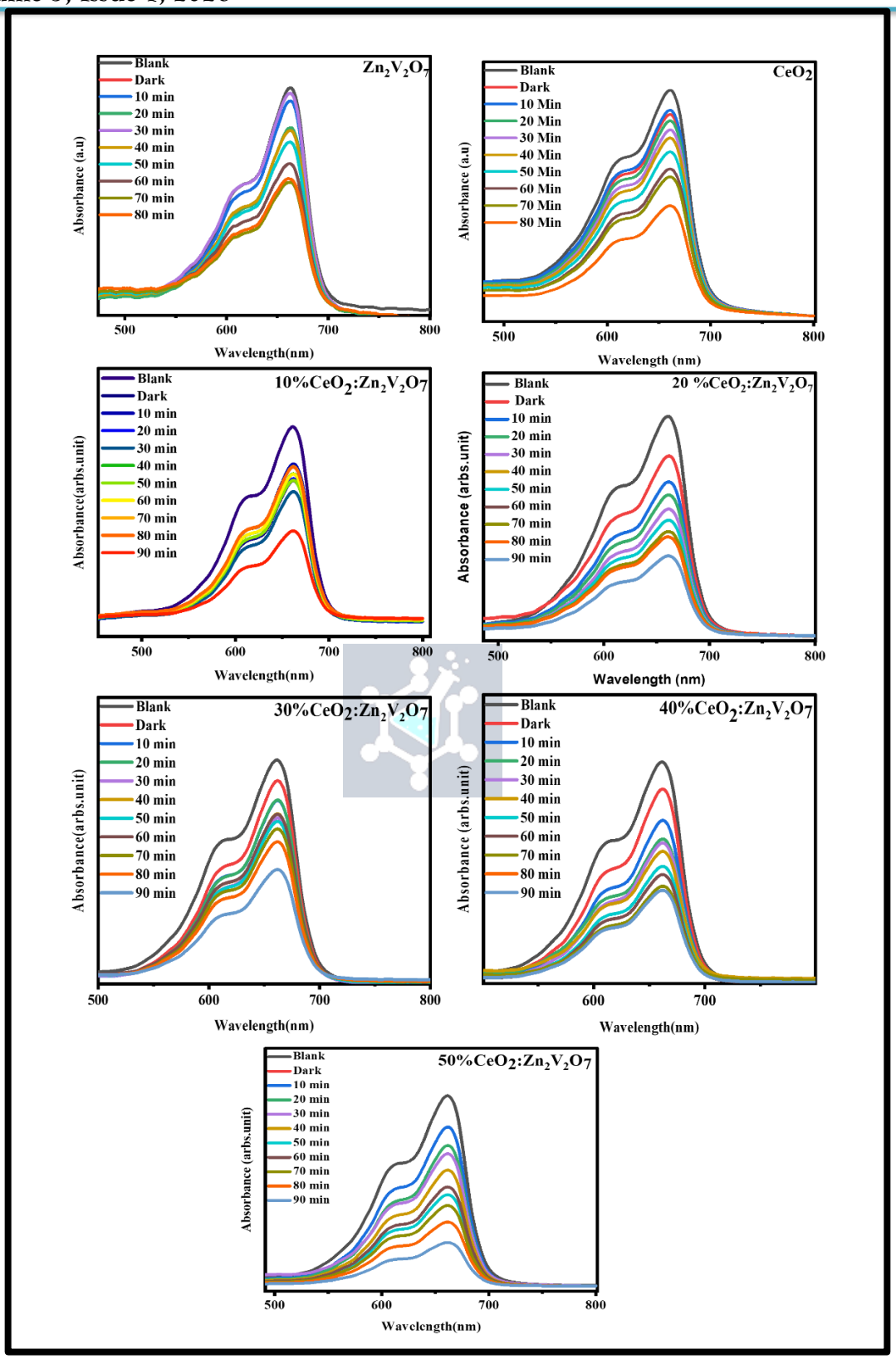

Figure 5. Photocatalytic results of Pure CeO2, Zn2V2O7 and their composites.

Journal of Chemical Research and Innovation
ISSN: 3106-7905 | 3106-7891
Volume 3, Issue 1, 2026

2.5. SEM Analysis

Scanning Electron Microscopy (SEM) was employed to examine the morphology and microstructure of pure CeO2, pure Zn2V2O7, and their hetero-doped nanocomposites. Zn2V2O7 exhibited interconnected nanosheets, while CeO2 consisted of agglomerated nanoparticles. CeO2 nanoparticles were immobilized on the surface of the 3D Zn2V2O7 framework, forming a well-defined heterojunction. With d-spacing values of 0.31 nm and 0.255 nm, respectively, high-resolution imaging showed two different kinds of lattice fringes that corresponded to the crystal planes of CeO2 and the (122) plane of Zn2V2O7. This confirmed the presence of a heterojunction, facilitating charge migration at the interface. Elemental mapping in Figure 6 demonstrated the uniform distribution of Ce, V, O, and Zn within the observed region. The SEM results reveal the successful construction of a 0D/3D CeO2/ **Zn2V2O7 heterojunction hybrid.**

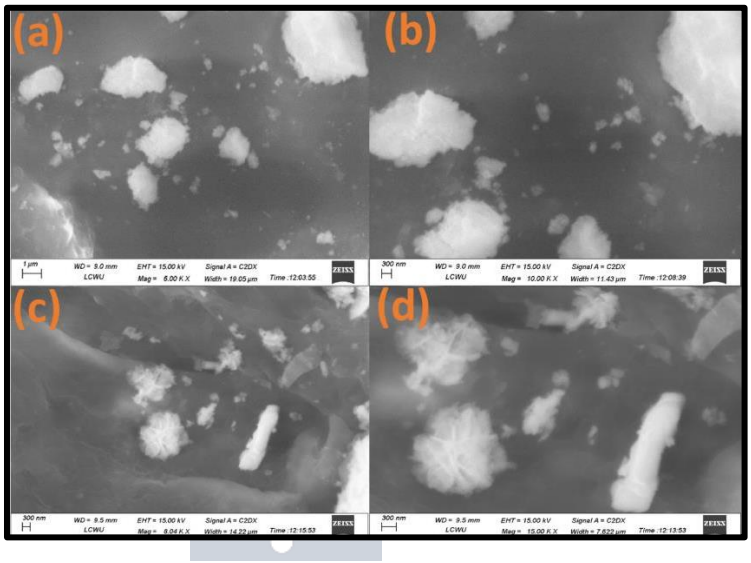

Figure 6. SEM Analysis of (a)CeO2 (b)Zn2V2O7(C)50% CeO2:Zn2V2O7(d)50% CeO2:Zn2V2O7

3. CONCLUSION

This study successfully synthesized and characterized CeO2/Zn2V2O7 nanocomposites, confirming their structural integrity and enhanced photocatalytic performance. XRD and FTIR analyses verified phase purity, while SEM revealed a well-defined heterojunction facilitating charge separation. UV-visible spectroscopy indicated that Ce doping influenced the electronic structure, improving light absorption. Photocatalytic experiments demonstrated superior methylene blue degradation, with complete degradation achieved in 90 minutes, attributed to efficient charge carrier migration and reduced recombination. These findings highlight the potential of CeO2/Zn2V2O7 heterojunctions as effective photocatalysts for environmental remediation.

REFERENCE

P. Gu *et al.*, "Recent advances in layered double hydroxide-based nanomaterials for the removal of radionuclides from aqueous solution," *ElsevierP Gu, S Zhang, X Li, X Wang, T Wen, R Jehan, A Alsaedi, T Hayat, X Wang Environmental pollution, 2018 • Elsevier*, Accessed: Dec. 01, 2024. [Online].

R. Ma *et al.*, "Comparative Investigation of Fe2O3 and Fe1- xS Nanostructures for uranium decontamination," *ACS Appl Nano Mater*, vol. 1, no. 10, pp. 5543–5552, Oct. 2018, doi: 10.1021/ACSANM.8B01059.

P. Gu *et al.*, "Experimental and theoretical calculation investigation on efficient Pb(II) adsorption on etched Ti3AlC2 nanofibers and nanosheets," *Environ Sci Nano*, vol. 5, no. 4, pp. 946–955, Apr. 2018, doi: 10.1039/C8EN00029H.

C. C. Wang, J. R. Li, X. L. Lv, Y. Q. Zhang, and G. Guo, "Photocatalytic organic pollutants degradation in metal–organic frameworks," *Energy Environ Sci*, vol. 7, no. 9, pp. 2831–2867, Aug. 2014, doi: 10.1039/C4EE01299B.

Y. L. Pang, A. Z. Abdullah, and S. Bhatia, "Review on sonochemical methods in the presence of catalysts and chemical additives for treatment of organic pollutants in wastewater," *Desalination*, vol. 277, no. 1–3, pp. 1–14, Aug. 2011, doi: 10.1016/J.DESAL.2011.04.049.

S. Norzaee, M. Taghavi, ... B. D.-J. of environmental, and undefined 2018, "Degradation of Penicillin G by heat activated persulfate in aqueous solution," *ElsevierS Norzaee, M Taghavi, B Djahed, FK MostafapourJournal of environmental management, 2018 • Elsevier*, Accessed: Dec. 21, 2024. [Online]. Available: https://www.sciencedirect.com/science/article/pii/S0301479718302652?

N. Zhang, J. Chen, Z. Fang, E. T.-C. E. Journal, and undefined 2019, "Ceria accelerated nanoscale zerovalent iron assisted heterogenous Fenton oxidation of tetracycline," *ElsevierN Zhang, J Chen, Z Fang, EP TsangChemical Engineering Journal, 2019 • Elsevier*, Accessed: Dec. 21, 2024. [Online]. Available: https://www.sciencedirect.com/science/article/pii/S1385894719305777?casa_token=9XRzVnYUj8MAAAAA:DXoaTpgk1KAAkxedlUKYEeEzakx26zITjt3XfjvPH_eY_DfhQK8ZuAlzQZoqpP0Ct MHHa46xww

M. Lekota, K. Dimpe, P. N.-J. of A. Science, and undefined 2019, "MgO-ZnO/carbon nanofiber nanocomposite as an adsorbent for ultrasound-assisted dispersive solid-phase microextraction of carbamazepine from wastewater prior to," *SpringerMW Lekota, KM Dimpe, PN NomngongoJournal of Analytical Science and Technology, 2019 • Springer*, vol. 10, no. 1, Dec. 2019, doi: 10.1186/s40543- 019-0185-1.

S. Zhang *et al.*, "Porous magnetic carbon sheets from biomass as an adsorbent for the fast removal of organic pollutants from aqueous solution," *pubs.rsc.orgS Zhang, M Zeng, J Li, J Li, J Xu, X WangJournal of Materials Chemistry A, 2014 • pubs.rsc.org*, doi: 10.1039/c0xx00000x.

I. M. Bulai and E. Venturino, "Biodegradation of organic pollutants in a water body," *J Math Chem*, vol. 54, no. 7, pp. 1387–1403, Aug. 2016, doi: 10.1007/S10910-016-0603-1/FIGURES/8.

Y. Yao *et al.*, "Fe, Co, Ni nanocrystals encapsulated in nitrogen-doped carbon nanotubes as Fenton- like catalysts for organic pollutant removal," *J Hazard Mater*, vol. 314, pp. 129–139, Aug. 2016, doi: 10.1016/J.JHAZMAT.2016.03.089.

D. Medeiros De Araújo, P. Cañizares, C. A. Martínez-Huitle, and M. A. Rodrigo, "Electrochemical conversion/combustion of a model organic pollutant on BDD anode: Role of sp3/sp2 ratio," *Electrochem commun*, vol. 47, pp. 37–40, Oct. 2014, doi: 10.1016/J.ELECOM.2014.07.017.

I. Tbessi *et al.*, "Effect of Ce and Mn co-doping on photocatalytic performance of sol-gel TiO2," *Solid State Sci*, vol. 88, pp. 20–28, Feb. 2019, doi: 10.1016/J.SOLIDSTATESCIENCES.2018.12.004.

I. K. Konstantinou and T. A. Albanis, "TiO2-assisted photocatalytic degradation of azo dyes in aqueous solution: kinetic and mechanistic investigations: A review," *Appl Catal B*, vol. 49, no. 1, pp. 1–14, Apr. 2004, doi: 10.1016/J.APCATB.2003.11.010.

U. I. Gaya and A. H. Abdullah, "Heterogeneous photocatalytic degradation of organic contaminants over titanium dioxide: A review of fundamentals, progress and problems," *Journal of Photochemistry and Photobiology C: Photochemistry Reviews*, vol. 9, no. 1, pp. 1–12, Mar. 2008, doi: 10.1016/J.JPHOTOCHEMREV.2007.12.003.

J. Wen, J. Xie, X. Chen, and X. Li, "A review on g-C3N4-based photocatalysts," *Appl Surf Sci*, vol. 391, pp. 72–123, Jan. 2017, doi: 10.1016/J.APSUSC.2016.07.030.

S. N. Frank and A. J. Bard, "Semiconductor Electrodes. 12. Photoassisted Oxidations and Photoelectrosynthesis at Polycrystalline TiO2 Electrodes," *J Am Chem Soc*, vol. 99, no. 14, pp. 4667– 4675, 1977, doi: 10.1021/JA00456A024/ASSET/JA00456A024.FP.PNG_V03.

M. Fernandes, K. R. Singh, ... T. S.-A. M., and undefined 2020, "Recent applications of magnesium oxide (MgO) nanoparticles in various domains," *aml.iaamonline.orgM Fernandes, K RB Singh, T Sarkar, P Singh, R Pratap SinghAdvanced Materials Letters, 2020 • aml.iaamonline.org*, Accessed: Dec. 21, 2024. [Online]. Available: https://aml.iaamonline.org/article_14017.html

M. Ahmaruzzaman, "Biochar based nanocomposites for photocatalytic degradation of emerging organic pollutants from water and wastewater," *Mater Res Bull*, vol. 140, p. 111262, Aug. 2021, doi: 10.1016/J.MATERRESBULL.2021.111262.

D. Mohanta, A. Mahanta, S. R. Mishra, S. Jasimuddin, and M. Ahmaruzzaman, "Novel SnO2@ZIF- 8/gC3N4 nanohybrids for excellent electrochemical performance towards sensing of p-nitrophenol," *Environ Res*, vol. 197, p. 111077, Jun. 2021, doi: 10.1016/J.ENVRES.2021.111077.

V. Gadore and M. Ahmaruzzaman, "Tailored fly ash materials: A recent progress of their properties and applications for remediation of organic and inorganic contaminants from water," *Journal of Water Process Engineering*, vol. 41, p. 101910, Jun. 2021, doi: 10.1016/J.JWPE.2020.101910.

M. Ahmaruzzaman and S. R. Mishra, "Photocatalytic performance of g-C3N4 based nanocomposites for effective degradation/removal of dyes from water and wastewater," *Mater Res Bull*, vol. 143, p. 111417, Nov. 2021, doi: 10.1016/J.MATERRESBULL.2021.111417.

J. T. Dahle and Y. Arai, "Environmental Geochemistry of Cerium: Applications and Toxicology of Cerium Oxide Nanoparticles," *International Journal of Environmental Research and Public Health 2015, Vol. 12, Pages 1253-1278*, vol. 12, no. 2, pp. 1253–1278, Jan. 2015, doi: 10.3390/IJERPH120201253.

J. Liu *et al.*, "Enhanced Gas Sensing Properties of SnO2 Hollow Spheres Decorated with CeO2 Nanoparticles Heterostructure Composite Materials," *ACS Appl Mater Interfaces*, vol. 8, no. 10, pp. 6669–6677, Mar. 2016, doi: 10.1021/ACSAMI.6B00169/SUPPL_FILE/AM6B00169_SI_001.PDF.

R. Zhao, L. Huan, P. Gu, R. Guo, M. Chen, and G. Diao, "Yb,Er-doped CeO2 nanotubes as an assistant layer for photoconversion-enhanced dye-sensitized solar cells," *J Power Sources*, vol. 331, pp. 527–534, Nov. 2016, doi: 10.1016/J.JPOWSOUR.2016.09.039.